Catalytic Methanation of Carbon Dioxide by Active Oxygen Material $Ce_xZr_{1-x}O_2$ Supported Ni—Co Bimetallic Nanocatalysts

Hongwei Zhu, Rauf Razzaq, Chunshan Li, Yaseen Muhmmad, and Suojiang Zhang
Beijing Key Laboratory of Ionic Liquids Clean Process, State Key Laboratory of Multiphase Complex System, Institute of Process Engineering, Chinese Academy of Sciences, Beijing 100190, P.R. China

DOI 10.1002/aic.14026
Published online February 14, 2013 in Wiley Online Library (wileyonlinelibrary.com)

A series of active oxygen material $Ce_xZr_{1-x}O_2$-supported Ni—Co bimetallic nanosized catalysts were prepared by coprecipitation method, which is simple and fit for industrial use with lower cost than other methods. The effect of CeO_2/ZrO_2 mole ratio, Co metal addition, and PEG-6000 addition were investigated. The catalysts were characterized through X-ray diffraction, H_2 thermal-programmed reduction, N_2 adsorption, Raman spectroscopy, CO pulse chemisorption, X-ray photoelectron spectroscopy, oxygen storage capacity, and transmission electron microscopy-energy dispersive X-ray analysis. Modifications of the structural and redox properties of these materials were evaluated in relation to their catalytic performances. Particularly, the relationship between the active oxygen sites of the catalysts and their catalytic performances was investigated. The interaction between active metals (Ni and Co) and $Ce_xZr_{1-x}O_2$ support was found to be very important for catalytic performance. The active oxygen site of $Ce_xZr_{1-x}O_2$ can considerably improve catalytic performance. Appropriate Co metal addition also remarkably enhanced the catalytic stability and activity. Moreover, PEG-6000 addition can improve the Brunauer–Emmett–Teller surface area and active metal dispersion of catalysts to improve their performances. The nanosized catalyst 15 wt % Ni-5 wt % Co/$Ce_{0.25}Zr_{0.75}O_2$ prepared by adding 5 wt % PEG-6000 achieved almost 85% CO_2 conversion and 98% selectivity to methane at 280°C when the gas hourly space velocity was 10,000 h^{-1}. © 2013 American Institute of Chemical Engineers *AIChE J*, 59: 2567–2576, 2013
Keywords: CO_2 methanation, active oxygen material, $Ce_xZr_{1-x}O_2$, Ni—Co bimetallic, nanosized catalysts

Introduction

CO_2 emission from human activities is one of the primary reasons for rapid global warming. In recent years, intensive efforts have been exerted for the development of new CO_2 fixation technologies. In this regard, catalytic CO_2 methanation for the synthesis of fuels and valuable products has attracted considerable interest.[1,2] Numerous supported catalysts based on group VIII (noble metals) based supported catalysts have been tested for CO_2 methanation.[3–7] Notably, Ni catalysts supported on oxide supports were most widely applied attributed to their higher activity and selectivity.[8–10] Support affects catalytic properties by manipulating the interaction between the active phase and support, thereby improving the attraction capacity of catalysts.

CeO_2–ZrO_2 solid solution ($Ce_xZr_{1-x}O_2$) has been commonly used as support for automotive three-way catalysts because of its high oxygen storage capacity (OSC), which is important in many reactions.[11–13] Several studies have found that active oxygen sites (oxygen vacancies) can interact with active metals to improve the performances of the catalysts.[14,15] Thus, CeO_2–ZrO_2 solid solution can be used as support for CO_2 methanation catalysts. Ni-based catalysts supported on $Ce_xZr_{1-x}O_2$ mixed oxides prepared by the sol-gel method have been previously investigated for CO_2 methanation.[16,17] Research shows that Ni-based catalysts on $Ce_xZr_{1-x}O_2$ mixed oxides are greatly efficient in terms of activity and stability, which can be attributed to their high oxygen storage capacities and high Ni dispersion. Ni^{2+} cation can get into the $Ce_xZr_{1-x}O_2$ structure and improve the redox properties of the material and restrict metal sintering, improving their catalytic performance. The proportion between Ni^{2+} cations incorporated into the CZ fluorite structure and surface Ni^0 in catalysts can be changed by the composition of CeO_2/ZrO_2 in supports. Many studies[18–20] have found that Co-based catalysts under low degree of reduction and increased amount of Co^{2+} active sites demonstrate higher catalytic activities for methanation, CH_4 selectivity, and poor selectivity towards long chain hydrocarbon-based liquid fuels. Thus, an oxidized Co state is more active toward the formation of methane at low temperatures, which proved our before research and Co addition can remarkably change the catalytic performances of $Ce_xZr_{1-x}O_2$ supported Ni catalysts. Many studies[21,22] used the coprecipitation method to prepare the support materials including $Ce_xZr_{1-x}O_2$ by adding the polyethylene glycol (PEG) as surfactant and dispersant. These researches find that PEG addition can improve the catalytic properties of these materials. For example, the PEG addition can increase the Brunauer, Emmett, Teller (BET) surface area

Correspondence concerning this article should be addressed to: C. Li or S. Zhang at csli@home.ipe.ac.cn or sjzhang@home.ipe.ac.cn.

of materials and prevent coagulation of particles in materials. In this study, a series of $Ce_xZr_{1-x}O_2$-supported Ni—Co bimetallic nanosized catalysts was prepared via coprecipitation method. The effect of CeO_2/ZrO_2 molar ratio, Co addition, and PEG-6000 addition was investigated. The catalysts were subsequently characterized using X-ray diffraction (XRD), thermal-programmed reduction (TPR), BET, Raman spectroscopy, CO pulse chemisorption, X-ray photoelectron spectroscopy (XPS), OSC, and transmission electron microscopy-energy dispersive X-ray analysis (SEM-EDX). Modifications of the structural and redox properties of these materials were correlated to their catalytic performances with special focus on the relationship between the active oxygen and catalytic performance. The interaction between active metals (Ni and Co) and $Ce_xZr_{1-x}O_2$ was found to be very important for catalytic performance. The active oxygen site of $Ce_xZr_{1-x}O_2$ can considerably improve the catalytic performance. Appropriate Co metal addition can increase both the catalytic stability and activity while further Co addition shows a negative effect. PEG-6000 addition can improve the BET surface area and active metal dispersion leading to enhanced performances.

Experimental Section

Catalyst *preparation*

$Ce_xZr_{1-x}O_2$ (CeO_2, $Ce_{0.8}Zr_{0.2}O_2$, $Ce_{0.5}Zr_{0.5}O_2$, $Ce_{0.25}Zr_{0.75}O_2$, $Ce_{0.2}Zr_{0.8}O_2$, and ZrO_2, in terms of molar composition) supported Ni-based bimetallic catalysts were prepared by coprecipitation method. Ni loading was 15 wt %, and Co doping was fixed at 5 and 10 wt %. $(NH_4)_2Ce(NO_3)_6$, $ZrOCl_2$, $Co(NO_3)_2$—$6H_2O$, and $Ni(NO_3)_2$—$6H_2O$ were used as metal precursors for Ce, Co, and Ni, respectively. PEG-6000 was then added into the metal precursor solution under different proportions (0, 5, and 10 wt %). The pH was maintained at approximately 9.5 by adding 0.2 mol L^{-1} aqueous KOH solution. The slurry was stirred vigorously for 2 h and aged for 2 h. After filtration and washing with water and alcohol until no Cl^- was detected by 0.1 M $AgNO_3$ solution, the solid was dried at 120°C for 12 h followed by calcination in air at 600°C for 4 h.

The catalysts were designated as 15Ni—zCo—$Ce_xZr_{1-x}O_2$—Py, where z is the mass concentration of Co (0, 5, and 10 wt %) and y is the mass concentration of PEG-6000 added (0, 5, and 10 wt %).

Catalyst characterization

XRD was performed using a Bruker AXS D8 Focus X-ray diffractometer with Ni-filtered Cu Kα radiation between 15° and 90°. Transmission electron microscopy (TEM) was performed by a JEM-2010 at an acceleration voltage of 200 kV. The samples were prepared by ultrasonic dispersion in acetone with a drop of the resultant suspension evaporated onto a holey carbon-supported grid. The BET surface area and pore structures were determined from the adsorption–desorption of nitrogen at liquid nitrogen temperature using Quadrasorb SI-MP equipment (Quantachrome, UK).

H_2-TPR was determined using a Micromerit Autochem II 2920. The catalyst was pretreated by passing Ar gas with a subsequent flow of 10% H_2/He at 499.85°C with 5°C min^{-1} heating rate. The amounts of chemisorbed CO were determined through a pulse method using Micromerit Autochem II 2920. After the catalysts were reduced *in situ* at 700°C for 1 h with H_2, pulses of 1% CO in He gas were injected through the catalysts at room temperature until no further adsorption of CO was detected using a thermal conductivity detector. XPS data were obtained using an ESCALab220i-XL electron spectrometer (VG Scientific) with 300 W A-Kα radiation. The base pressure was approximately 3×10^{-9} mbar. The binding energies were referenced to the C1s line at 284.8 eV from adventitious carbon. Raman spectroscopy was recorded by Lab-Ram HR 800 spectrometer (Jobin Yvon-Horiba) with 514.53 nm of an Ar–Kr 2018 RM laser (Spectrum Physics) as the excitation source. The OSC was measured through the CO-pulse technique using a GC-6860 chromatograph (Shandong Ruihong Instrument Co. Ltd., China). The sample was first oxidized with a 10% O_2/He flow of 50 mL min^{-1} at 850°C for 10 min. This was followed by He stream purging for another 10 min. A 1 mL pulse of pure CO was then injected into the system, and oxygen storage was determined by the amount of CO_2 produced.

Determination of catalytic activity

The catalysts were reduced *in situ* before the reaction under a pure H_2 stream for 3 h with a total gas flow of 50 mL min^{-1} at 350°C with 5°C min^{-1} heating rate. Catalytic activity tests were performed in a fixed-bed quartz tubular reactor (10 mm I.D.) at 2 MPa pressure. The catalyst was sieved and selected in 200–315 μm fractions. The volume of each catalyst was 1.0 mL. A gas mixture containing 16.36% CO_2, 18.19% N_2 (internal standard), and 65.45% H_2 was continuously passed through the catalysts at a space velocity of 5000 h^{-1}. CO_2 conversion and CH_4 selectivity were defined as follows:

$$\mathrm{CO_2\ conversion}: X_{CO_2}(\%) = \left(\frac{[M_{CO_2}]_{In} - [M_{CO_2}]_{Out}}{[M_{CO_2}]_{In}}\right) \times 100$$

$$\mathrm{CH_4\ selectivity}\, S_{CH_4}(\%) = \left(\frac{[M_{CH_4}]_{Out} - [M_{CH_4}]_{In}}{[M_{CO_2}]_{In} - [M_{CO_2}]_{Out}}\right) \times 100$$

where M is the molar concentration of the inlet and outlet species and S is the CH_4 selectivity with respect to CO and CO_2. The X_{CO_2} of active metals on the surface of catalysts was used to calculate the reaction rate as:

$$r_{CO_2} = \frac{N_{CO_2} * X_{CO_2}}{N_{metal(surface)}}$$

where N_{CO_2} is the CO_2 molar gas flow rate in mol/s, $N_{Ni(surface)}$ is the molar of Ni and Co on the surface of catalyst which were detected by the amounts of chemisorbed CO, and r_{CO_2} is the reaction rate of Ni and Co on the surface of catalyst. Thermodynamic equilibrium calculations were performed at various temperatures ranging from 200 to 400°C by a process simulation equilibrium reactor program (Aspen Plus V7.0) to compare our catalytic results to thermodynamic limitations.

Results

BET and pore structures

The texture properties of the different catalysts are shown in Table 1. When the Ni and Co loadings were fixed at 15 and 5 wt %, respectively, ZrO_2 addition into CeO_2 increased the BET surface area of the catalysts. For instance, an increase from 0 to 0.5 (mole ratio) of ZrO_2 contents correspondingly increased BET surface area from 67 to 81 m^2 g^{-1}. However, further addition of ZrO_2 caused a

Table 1. Texture Properties of the Different $Ce_xZr_{1-x}O_2$ Supported Ni—Co Bimetallic Catalysts

Catalyst	Co content (wt %)	PEG-6000 content (wt %)	Surface srea ($m^2\ g^{-1}$)	Average pore diameter (nm)	Total pore volume ($cm^3\ g^{-1}$)
15Ni—5Co/$Ce_1Zr_0O_2$	5	–	67	2.62	0.063
15Ni—5Co/$Ce_{0.8}Zr_{0.2}O_2$	5	–	74	2.26	0.072
15Ni—5Co/$Ce_{0.5}Zr_{0.5}O_2$	5	–	81	1.97	0.075
15Ni—5Co/$Ce_{0.25}Zr_{0.75}O_2$	5	–	78	2.05	0.068
15Ni—5Co/$Ce_{0.2}Zr_{0.8}O_2$	5	–	70	2.31	0.064
15Ni—5Co/$Ce_{0.1}Zr_{0.9}O_2$	5	–	62	3.07	0.053
15Ni—5Co/$Ce_0Zr_1O_2$	5	–	58	3.10	0.051
15Ni—0Co/$Ce_{0.25}Zr_{0.75}O_2$	0	–	75	2.33	0.069
15Ni—10Co/$Ce_{0.25}Zr_{0.75}O_2$	10	–	56	3.12	0.050
15Ni—5Co/$Ce_{0.25}Zr_{0.75}O_2$—P5	5	5	108	1.78	0.082
15Ni— 5Co/$Ce_{0.25}Zr_{0.75}O_2$—P10	5	10	60	1.71	0.061

decrease in BET surface area, the surface area of 15Ni—5Co/$Ce_{0.1}Zr_{0.9}O_2$ decreased to 62 $m^2\ g^{-1}$. The BET surface area of 15Ni—5Co/$Ce_{0.5}Zr_{0.5}O_2$ was almost equal to that of 15Ni—0Co/$Ce_{0.5}Zr_{0.5}O_2$. When the Co loading was increased to 10 wt %, the BET surface area decreased to 56 $m^2\ g^{-1}$. The addition of 5 wt % PEG-6000 into the catalyst increased the BET surface area from 78 to 108 $m^2\ g^{-1}$. However, by increasing PEG-6000 content to 10 wt %, the BET surface area decreased to 60 $m^2\ g^{-1}$.

XRD results

Figure 1 shows the XRD patterns of the catalysts with different ZrO_2 to CeO_2 mole ratios, in which the Ni and Co loadings were 15 and 5 wt %. The XRD patterns of 15Ni—5Co/$Ce_1Zr_0O_2$ catalyst without ZrO_2 can be readily indexed to those of a CeO_2 cubic phase. With increased ZrO_2 content in the catalysts, all peaks in the XRD patterns slightly shift to larger angle, confirming the formation of homogenous $Ce_{1-x}Zr_xO_2$ solid solutions. Diffraction peaks corresponding to NiO can be detected in all catalysts.

The XRD patterns of the catalysts with different Co loadings are shown in Figure 2. When the Co loading was increased from 0 to 5 wt %, the XRD patterns of the catalyst did not considerably change. Further increase Co loading to 10 wt % caused a strong diffraction peaks of NiO and the Co_3O_4 diffraction peaks can also be detected.

The XRD patterns of the 15Ni—5Co/$Ce_{0.25}Zr_{0.75}$ catalysts prepared by adding different amounts of PEG-6000 are shown in Figure 3. The addition of 5 wt % PEG-6000 into the catalyst weakened the NiO diffraction peak, whereas 10 wt % PEG-6000 addition showed a reverse effect.

TEM and EDX

Figures 4 and 5 showed the TEM images and EDX results of the 15Ni—5Co/$Ce_{0.25}Zr_{0.75}O_2$—P5 catalysts, which was found to consist of nanospheres (diameter 20–30 nm). The EDX results showed that the weight ratio of Ni to Co was three confirming the designed composition. The same was true for Ce to Zr mole ratio as well. By contrast, the weight ratio of Ni to Zr was remarkably higher than that of the designed composition, which indicated that active metal Ni and Co were more abundant on the surface of the catalysts than inside of the catalysts.

TPR analysis

The TPR profiles of different catalysts are shown in Figure 6. In previous studies, the peaks corresponding to the reduction of NiO to Ni were observed at 300–550°C.[23,24] Two continuous peaks were observed, that is, at 220–380°C and 400–580°C corresponding to the reduction of Co_3O_4 to CoO and CoO to metallic Co, respectively. The peak intensity of 15Ni—0Co—$Ce_{0.25}Zr_{0.75}O_2$ at low temperatures was very low because of the reduction of NiO on catalyst surface. In addition, this catalyst did not strongly interact with support. The peaks observed at approximately 300–550°C can be attributed

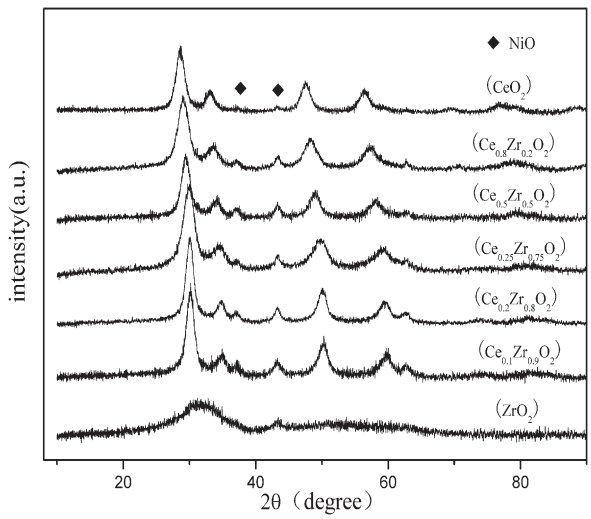

Figure 1. XRD patterns of the catalysts with different mole ratio of ZrO_2 to CeO_2.

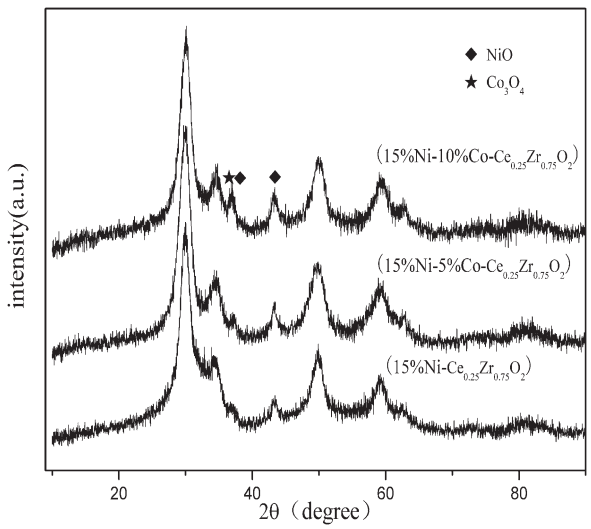

Figure 2. XRD patterns of the catalysts supported on $Ce_{0.25}Zr_{0.75}O_2$ with different Co loading.

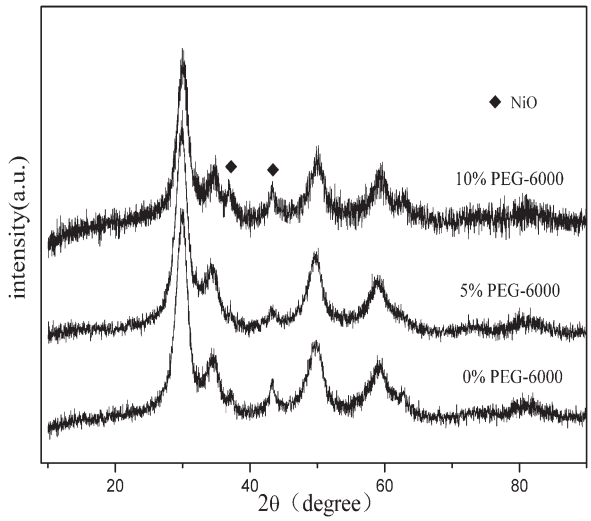

Figure 3. XRD patterns of the 15Ni—5Co/$Ce_{0.25}Zr_{0.75}O_2$ catalysts prepared by adding different content of PEG-6000.

to NiO reduction, which highly interacted with support and substituted Zr^{4+} or Ce^{4+}. The low temperature reduction peak of 15Ni—5Co/CeO_2 was remarkably higher than that of 15Ni—5Co/ZO_2, but its high-temperature peak was much lower than that of 15Ni—5Co/ZO_2. The results show that 15Ni—5Co/CeO_2 was easier to be reduced than 15Ni—5Co/ZrO_2, and that more NiO strongly interacted with supports in the 15Ni—5Co/ZrO_2. The addition of ZrO_2 into CeO_2 can weaken the low-temperature reduction peaks and intensify the high-temperature peaks. Thus, the addition of ZrO_2 into the catalysts can decrease the quantity of NiO or Co_3O_4 on the catalyst surface and enhance the interaction between active metal and support. Meanwhile, a comparison of the TPR profiles between 15Ni—5Co/$Ce_{0.8}Zr_{0.2}O_2$ and 15Ni—5Co/$Ce_{0.25}Zr_{0.75}O_2$ suggested that increased ZrO_2 content strengthened the reduction peaks at the high-temperature range. The addition of 5 wt % PEG-6000 to the catalyst increased the high-temperature reduction peaks only while did not change the low-temperature peaks, which also made the high-temperature reduction peaks shift to low temperature.

Raman spectroscopy

The Raman spectra of the different catalysts were shown in Figure 7. Six Raman peaks of symmetry centered at 147, 268, 313, 460, 600, and 645 cm^{-1} are observed in t-ZrO_2, whereas only one peak centered at approximately 465 cm^{-1} can be observed in cubic CeO_2.[25,26] NiO had a broad Raman band at approximately 500 cm^{-1}. Several peaks were found near 485, 520, 623, and 693 cm^{-1}, which were typical of Co_3O_4 phase with a cubic fluorite structure. In the Raman spectra of 15Ni—5Co/$Ce_{0.8}Zr_{0.2}O_2$, one peak was observed at approximately 465 cm^{-1} while many small peaks were found for t-ZrO_2, NiO, and Co_3O_4. These peaks were overlapped and were not obviously observed. However, the Raman spectra of catalysts showed a slight red shift and broadening of the peak at 465 cm^{-1} with increased ZrO_2 content. This phenomenon was a result of the increase in oxygen vacancies and the cell contraction caused by Zr^{4+} incorporation into the CeO_2 lattice, forming a solid solution with the cubic phase. This observation suggested the presence of more defective structures in 15Ni—5Co/$Ce_{0.25}Zr_{0.75}O_2$—P5 than in 15Ni— 5Co/$Ce_{0.8}Zr_{0.2}O_2$ because more Ce^{4+} were replaced by Zr^{4+}. Such defects favor electron transfer from the support to the active metal. If $Ce_xZr_{1-x}O_2$ contains more defects, then more active metal cations can incorporate into the $Ce_xZr_{1-x}O_2$ lattice for charge balance. The broadening of such peak can also be increased by the addition of Ni and Co oxide, which can also incorporate into the CeO_2 lattice to replace the Ce cations. The Raman peak at approximately 600 cm^{-1} can be attributed to the presence of intrinsic oxygen vacancies in the lattice.[27] Thus, 15Ni—5Co/$Ce_{0.25}Zr_{0.75}O_2$— P5 had more oxygen vacancies than 15Ni—5Co/$Ce_{0.8}Zr_{0.2}O_2$. A weak Raman band at approximately 1160 cm^{-1} can be observed in the Raman spectra of 15Ni—5Co—$Ce_{0.25}Zr_{0.75}O_2$—P5, which can be attributed to the presence of CeO_2 defects and more oxygen vacancies.[28] The intensity of the peak at approximately 1160 cm^{-1} became higher after the H_2 treatment.

OSC and CO chemisorption

The OSC and CO chemisorption results are shown in Table 2. The OSC of the catalyst mainly depend on the nature of the support. The OSC of the catalyst containing ZrO_2 was much higher than that of 15Ni— 5Co—CeO_2. The addition of ZrO_2

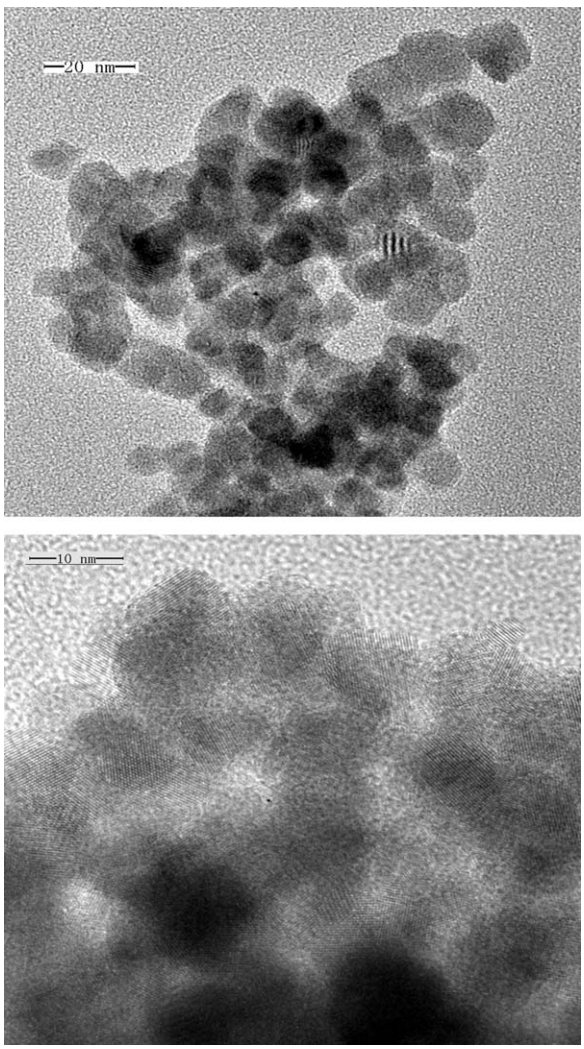

Figure 4. TEM of the 15Ni—5Co/$Ce_{0.25}Zr_{0.75}O_2$—P5 catalysts.

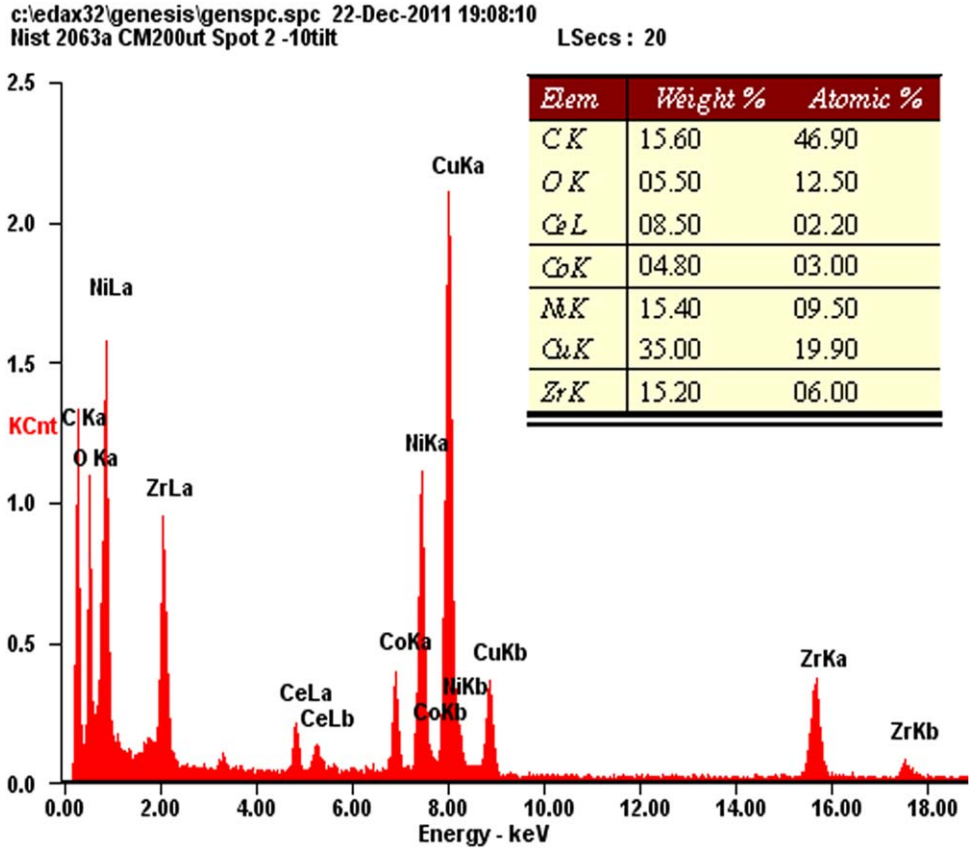

Figure 5. EDX results of the 15Ni—5Co/$Ce_{0.25}Zr_{0.75}O_2$—P5 catalysts.

[Color figure can be viewed in the online issue, which is available at wileyonlinelibrary.com.]

also increased the CO chemisorption of a catalyst, thereby improving the dispersion of active metals. The OSC of the catalyst is only slightly increased after the Co addition because less Co cations than Zr^{4+} can be inserted into the crystalline structure of CeO_2 to improve the OSC of the catalyst. However, the addition of Co addition can improved the CO chemisorption of the catalyst and hence increased the active metal dispersion. PEG-6000 addition can also simultaneously improved the OSC and CO chemisorption of the catalyst. Hence, the 15Ni—5Co—$Ce_{0.25}Zr_{0.75}O_2$—P5 nanocatalyst had the highest OSC, CO chemisorption, and active metal dispersion among all the studied catalysts.

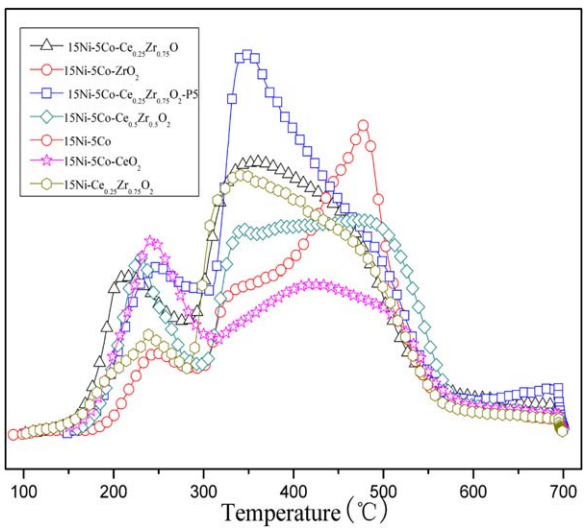

Figure 6. H_2-TPR spectra of different $Ce_xZr_{1-x}O_2$ supported Ni—Co bimetallic catalysts.

[Color figure can be viewed in the online issue, which is available at wileyonlinelibrary.com.]

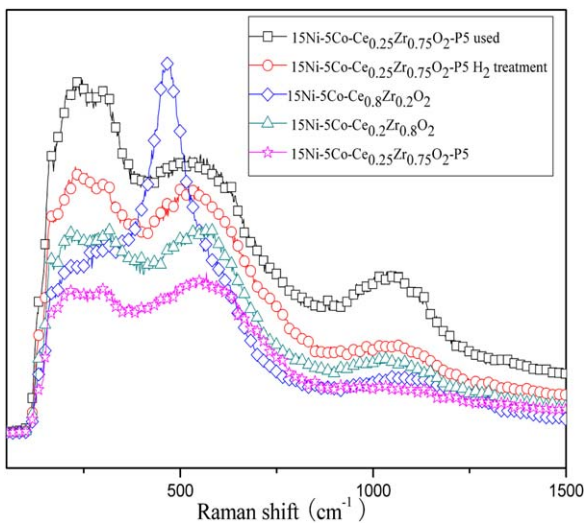

Figure 7. Raman spectra of different $Ce_xZr_{1-x}O_2$ supported Ni—Co bimetallic catalysts.

[Color figure can be viewed in the online issue, which is available at wileyonlinelibrary.com.]

Table 2. The OSC and CO Chemisorption Results of Different $Ce_xZr_{1-x}O_2$ Supported Ni—Co Bimetallic Catalysts

Catalyst	OSC (μmol g^{-1})	CO Chemisorption (%)
15Ni—5Co/CeO_2	456	15.6
15Ni—5Co/$Ce_{0.8}Zr_{0.2}O_2$	578	18.2
15Ni/$Ce_{0.25}Zr_{0.75}O_2$	656	15.2
15Ni—5Co/$Ce_{0.25}Zr_{0.75}O_2$	662	21.8
15Ni—5Co/$Ce_{0.25}Zr_{0.75}O_2$—P5	708	26.5
15Ni—5Co/$Ce_{0.25}Zr_{0.75}O_2$—P10	496	16.4

XPS studies

The XPS results of fresh and used (48 h) 15Ni—5Co—$Ce_{0.25}Zr_{0.75}O_2$—P5 catalyst are shown in Figure 8. The peaks at 855 and 852 of fresh 15Ni—5Co—$Ce_{0.25}Zr_{0.75}O_2$—P5 catalyst were assigned to Ni^{2+} and metallic Ni, respectively. In fresh catalyst, Ni^{2+} was the major form before H_2-treatment, and the peak slightly moved to lower binding energy, indicating an improvement in the reduction capacity of the catalyst. The Ni^{2+}/Ni^0 ratio increased, but a quantity of Ni^{2+} was still present in the catalyst. The Co 2 p XPS results showed that the Co 2 p peak position and shape were consistent with those of Co_3O_4. However, after H_2-treatment or use, Co_3O_4 was reduced to CoO. The reduction capacity of Co_3O_4 was higher than that of Ni^{2+}. Thus, Co_3O_4 was reduced first to hamper the reduction of Ni^{2+}. The O 1 s result revealed that the O 1 s peak position (530.10 eV) was caused by the M–O bonds, and a slight increment in the high binding energy (BE) tail suggested the formation of new hydroxyl groups on the supported oxide surface. The O^{2-} peak of the used catalyst tended to shift toward a higher BE than that of fresh catalyst. The transfer of the lattice oxygen in the catalyst to the catalyst surface can be attributed to the increase in the O 1 s binding energy.[29] Meanwhile, the higher binding energy shoulder can be attributed to the presence of oxygen vacancies or O^- species.[30]

Catalytic activity studies

Activities of Catalysts with Different CeO_2/ZrO_2 Mole Ratios. The resulting activities of the catalysts with different CeO_2/ZrO_2 mole ratios are illustrated in Figure 9. The addition of ZrO_2 to CeO_2 produced mixed oxides, which considerably improved the catalytic activities. Among the catalysts tested, 15Ni—5Co—$Ce_{0.25}Zr_{0.75}O_2$ showed the best catalytic performance, with nearly 90% CO_2 conversion at 320°C. Moreover, the catalytic activity of 15Ni—5Co— $Ce_{0.2}Zr_{0.8}O_2$ was lower than that of 15Ni— 5Co—$Ce_{0.25}Zr_{0.75}O_2$ indicating the negative effect of excess ZrO_2. Arrhenius plots for CO_2 methanation on catalysts with different mole ratio of ZrO_2 to CeO_2 was shown in Figure 10. The results showed that the apparent activation energy of the catalyst supported on the $Ce_{0.25}Zr_{0.75}O_2$ was the lowest, hence the rate of the catalyst supported on the $Ce_{0.25}Zr_{0.75}O_2$ was the highest among all the catalysts. When the molar ratio of ZrO_2 in the catalyst increased from 0 to 75%, the apparent activation energy of catalysts decreased, but when the molar ratio of ZrO_2 increased to 80, the apparent activation energy increased.

Activities of the Catalysts Added with Different Co Contents. The effect of different Co contents on catalytic activity is shown in Figure 11. A certain amount of Co can improve the catalysts activities. Thus, the activity of 15Ni—5Co/$Ce_{0.25}Zr_{0.75}O_2$ was better than that of the 15Ni—0Co/$Ce_{0.25}Zr_{0.75}O_2$. However, 10 wt % of Co addition in 15Ni— 0Co/$Ce_{0.25}Zr_{0.75}O_2$ causes a decrease in activity compared to 15Ni— 5Co/$Ce_{0.25}Zr_{0.75}O_2$, indicating that 5 wt % was the optimum level for Co addition. CO_2 conversion was also increased by the 5 wt % Co addition.

Activities of the Catalysts Added with Different PEG-6000 Contents. The activities of the catalysts added with different amounts of PEG-6000 are shown in Figure 12. The addition of 5 wt % PEG-6000 improved the activity of the catalysts, whereas 10 wt % addition induced a considerable decrease the activity of catalyst. Active metals dispersion on the surface of catalysts can be improved greatly. Thus, adding 5 wt % PEG-6000 improved the CO_2 conversion of catalysts. The catalytic activity of 15Ni—5Co/$Ce_{0.25}Zr_{0.75}O_2$— P5, which achieved almost 85% CO_2 conversion and 98% selectivity to methane at 280°C when the gas hourly space velocity was 10,000 h^{-1}, can approach the equilibrium conversion at 350°C.

Activities of Catalysts at Different Gas Hourly Space Velocity. The activities of the catalysts Ni—5Co / $Ce_{0.25}Zr_{0.75}O_2$—P5 at different gas hourly space velocities are shown in Figure 13. With increased gas hourly space velocity from 3000 to 10,000 h^{-1}, the activities of catalyst keep almost the same. As the gas hourly space velocity was increased to 20,000 h^{-1}, the activities of catalyst only slightly changed.

Long-Term Stability of Catalytic Activity. Figure 14 shows the long-term stability of the different catalysts, which was detected at 320°C for 120 h. Under these conditions, the CO_2 conversion efficiency of 15Ni—5Co/$Ce_{0.8}Zr_{0.2}O_2$ decreased to 49.5%, whereas that of 15Ni—5Co/$Ce_{0.25}Zr_{0.75}O_2$ slowly decreased slowly to 70.2% indicating a more stable activity. Comparing the results of 15Ni—5Co/$Ce_{0.25}Zr_{0.75}O_2$ with those of 15Ni—0Co/$Ce_{0.25}Zr_{0.75}O_2$, revealed that adding 5 wt % Co into catalysts also considerably improve the stability of catalysts. After used at 320°C for 120 h, the CO_2 conversion of 15Ni—5Co/$Ce_{0.25}Zr_{0.75}O_2$—5P decreased only to 76.8%, ranking it at the top of stability series among all the catalysts.

Discussion

$Ce_xZr_{1-x}O_2$ mixed oxides are widely used in three-way catalysts as oxygen storage materials. These oxides mainly

Table 3. The Properties of Different $Ce_xZr_{1-x}O_2$ Supported Ni—Co Bimetallic Catalysts

Catalyst	Surface area (m^2 g^{-1})	OSC (μmol g^{-1})	Particle size (nm)	CO Chemisorption (%)	Catalyst bulk Density (g cm^{-3})
15Ni—5Co/CeO_2	67	456	52	15.6	5.60
15Ni—5Co/$Ce_{0.8}Zr_{0.2}O_2$	74	578	48	18.2	5.56
15Ni/$Ce_{0.25}Zr_{0.75}O_2$	75	656	41	15.2	5.55
15Ni—5Co/$Ce_{0.25}Zr_{0.75}O_2$	78	662	40	21.8	5.52
15Ni—5Co/$Ce_{0.25}Zr_{0.75}O_2$—P5	108	708	35	26.5	5.45
15Ni—5Co/$Ce_{0.25}Zr_{0.75}O_2$—P10	60	496	53	16.4	5.64

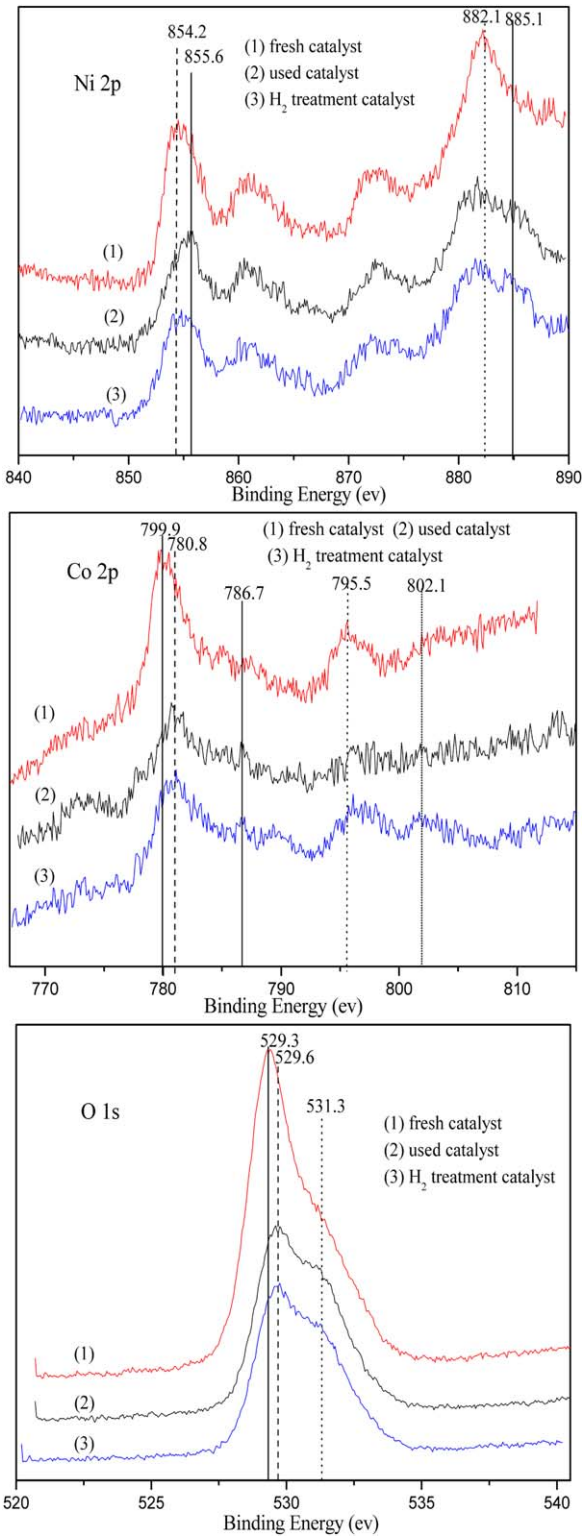

Figure 8. The XPS results of the fresh and used 15Ni—5Co/$Ce_{0.25}Zr_{0.75}O_2$—P5 catalyst (used for 48 h).

[Color figure can be viewed in the online issue, which is available at wileyonlinelibrary.com.]

act as an oxygen buffer by storing/releasing oxygen because of the rapid Ce^{4+}/Ce^{3+} redox process in solids. The Properties of different $Ce_xZr_{1-x}O_2$ supported Ni-Co bimetallic catalysts were showed in the Table 3. The CeO_2/ZrO_2 ratio is

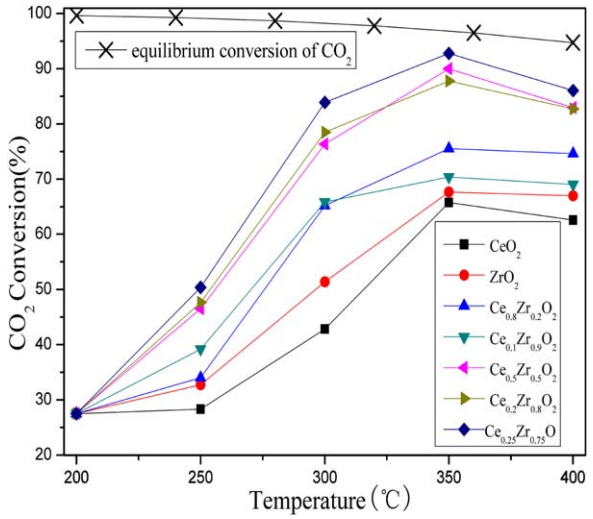

Figure 9. The catalytic activity of different catalysts with different mole ratio of ZrO_2 to CeO_2.

[Color figure can be viewed in the online issue, which is available at wileyonlinelibrary.com.]

one of the crucial factors affecting the OSC performance of $Ce_xZr_{1-x}O_2$.[31] A previous research[32] has shown that the oxygen migration channel in ZrO_2-rich tetragonal structure is larger than that in CeO_2-rich cubic structure. In the present study, the XRD patterns of catalysts matched the patterns change from the face centered cubic structure to the tetragonals structure with increased the molar ratio of ZrO_2. Studies[33,34] have shown that for metastable nanocrystals of $Ce_xZr_{1-x}O_2$, it is difficult to determine their crystal phase owing to their broadened XRD peaks. Raman spectroscopy can be used to distinguish between the cubic and tetragonal phases. The Raman spectra of $Ce_{0.5}Zr_{0.5}O_2$ and $Ce_{0.25}Zr_{0.75}O_2$ presented the characteristic F2g vibration mode of the fluorite-type structure, suggesting that both materials possessed a cubic structure. The cubic structure is more reducible than the pure tetragonal structure. The

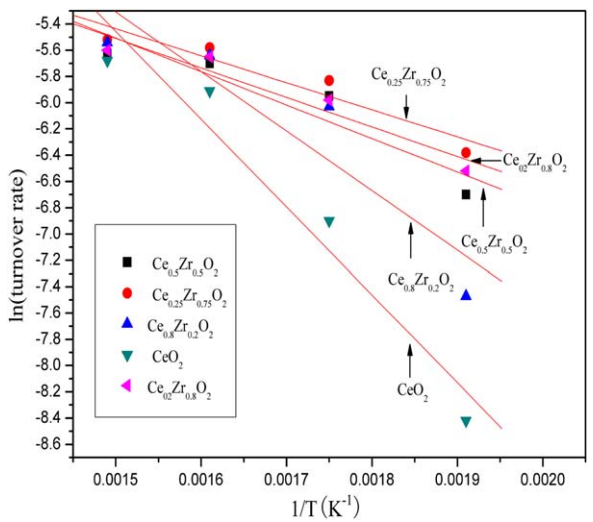

Figure 10. Arrhenius plots for CO_2 methanation on catalysts with different mole ratio of ZrO_2 to CeO_2.

[Color figure can be viewed in the online issue, which is available at wileyonlinelibrary.com.]

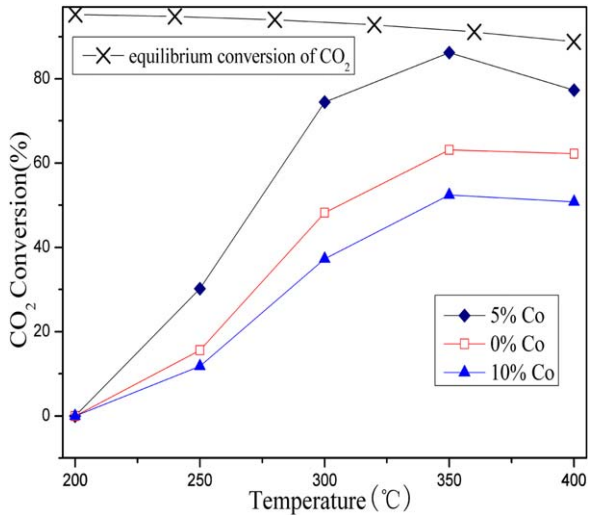

Figure 11. The catalytic activity of catalysts supported on $Ce_{0.25}Zr_{0.75}O_2$ with different Co loading.

[Color figure can be viewed in the online issue, which is available at wileyonlinelibrary.com.]

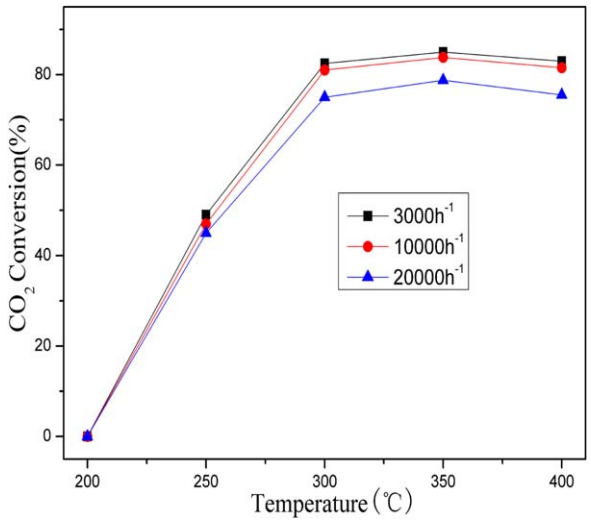

Figure 13. The catalytic activity of catalysts 15Ni—5Co/$Ce_{0.25}Zr_{0.75}O_2$—P5 at different gas hourly space velocity.

[Color figure can be viewed in the online issue, which is available at wileyonlinelibrary.com.]

presence of zirconia increases the oxygen mobility in the ceria lattice and increases the process of vacancy formation, making the material more reducible. CO_2 methanation was carried out using Ni—Co bimetallic nanocatalysts supported on $Ce_xZr_{1-x}O_2$ mixed oxides prepared by coprecipitation method. The CeO_2/ZrO_2 ratio affected the catalytic activity, and ZrO_2 was incorporated into the CeO_2 lattice to form mixed oxides. The BET surface area of a catalyst cannot be considerably improved by adding a certain amount of ZrO_2 while its excessive addition can even decrease it. The change in the catalytic performance was primarily due to the changes in its crystalline structure. In the CeO_2 cubic phase of $Ce_xZr_{1-x}O_2$ with ZrO_2 addition, the tetravalent cation Ce^{4+} has an eight-coordination of oxygen cations. Ce^{4+} can be replaced by Zr^{4+} or by divalent cations (Ni^{2+} and Co^{2+}) to obtain more oxygen vacancies directly increasing the active sites for many reactions.[35] A previous study[17] has found that the catalytic activity and stability of $Ce_xZr_{1-x}O_2$ supported Ni catalysts are highly influenced by CeO_2/ZrO_2 ratio of the mixed oxides. The CeO_2/ZrO_2 ratio can determine the proportion between Ni^{2+} cations incorporated into the fluorite structure and surface Ni^0 of $Ce_xZr_{1-x}O_2$ mixed oxides in the catalyst. The incorporation of Ni^{2+} into $Ce_xZr_{1-x}O_2$ mixed oxides can enhance its specific activity. Thus, in this study, the structure of $Ce_xZr_{1-x}O_2$ was significantly influenced by the ZrO_2 contents in the mixed oxides, as detected by XRD and Raman spectroscopy. The incorporation of ZrO_2 into the CeO_2 lattice improved the OSC of the catalyst and obtained more defects. Thus, more active metal cations can be incorporated into the lattice of $Ce_xZr_{1-x}O_2$ mixed oxides to improve the OSC and generate more surface defects. The interaction between $Ce_xZr_{1-x}O_2$

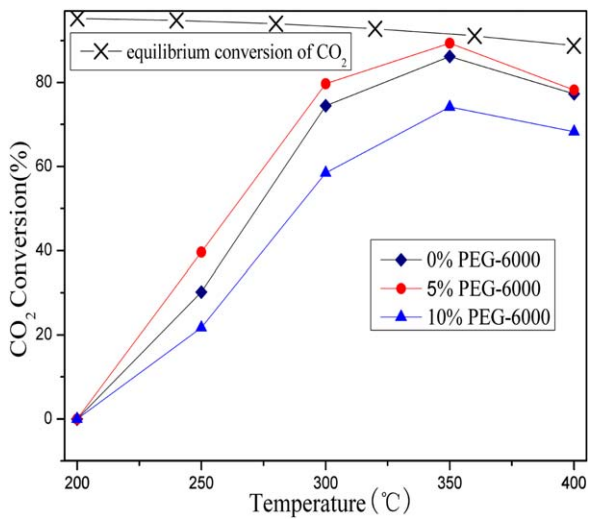

Figure 12. The catalytic activity of 15Ni—5Co/$Ce_{0.25}Zr_{0.75}O_2$ catalysts prepared by adding different content of PEG-6000.

[Color figure can be viewed in the online issue, which is available at wileyonlinelibrary.com.]

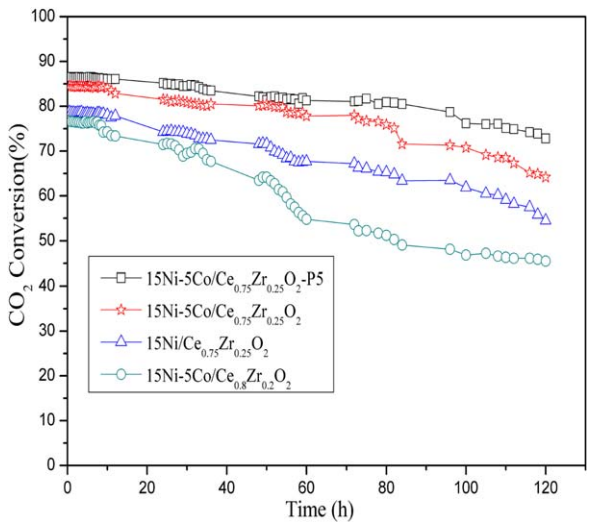

Figure 14. The catalytic activities for long-term time of the different catalysts.

[Color figure can be viewed in the online issue, which is available at wileyonlinelibrary.com.]

and active metals was very important for the catalytic performances. The catalytic activity and stability of 15Ni—5Co/$Ce_{0.75}Zr_{0.25}O_2$ were higher than those of other $Ce_xZr_{1-x}O_2$ supported Ni—Co bimetallic catalysts. The incorporation of Ni and Co can increase the surface atomic ratios of Ce/Zr, reducing a part of Ce^{4+} into Ce^{3+} to maintain the electrical neutrality or the formation of oxygen vacancies of $Ce_xZr_{1-x}O_2$ mixed oxides. The incorporation of active metals cations favored the transfer of oxygen in the catalysts.[36]

The oxidized Co state is more active toward the formation of methane at low temperatures,[18–20] and Co addition can remarkably change the catalytic performances of $Ce_xZr_{1-x}O_2$ supported Ni catalysts. The TPR results showed that Co addition significantly influenced the reduction capacity. Highly dispersed Co_3O_4 addition improved the redox properties by interacting with Ni and $Ce_xZr_{1-x}O_2$. Adding 5 wt % Co into the catalyst made the TPR of the reduction peaks shift to lower temperature and also considerably improved in CO_2 chemisorption. A previous study[37] have found that a homogeneous alloy of Co and Ni can be formed after H_2 reduction and remain after use for reaction in Co—Ni bimetallic catalysts, which can increased the metal dispersion in the catalyst. Thus, a certain amount of Co addition can considerably improve catalytic performance. But adding excessive Co(10 wt %) into catalysts decreased the BET surface area of the catalysts and made more reduced Co metal lie on catalyst surface. Reduced Co is highly active for the Fischer–Tropsch synthesis, which strongly attracts the CO obtained from CO_2 dissociation and hampers the methanation reaction. Thus, excessive Co was detrimental to the catalysts activities. Adding 5 wt % Co into catalysts can also considerably improve their stability. The cobalt-containing catalysts, showed substantially higher resistance to carbon deposition than Ni-based catalysts. Thus, Co is effective in preventing carbon deposition also in the presence of a strong chemical interaction with nickel to Co—Ni alloy.[38]

The TEM results showed that catalysts containing 5 wt % PEG-6000 consisted of a large quantity of nanospheres with diameters range of from 20 to 40 nm. The catalysts exhibited various characteristics of nanomaterials. The BET surface area was increased by adding 5 wt % PEG-6000. The coprecipitation method was used to prepare the support materials including $Ce_xZr_{1-x}O_2$ by adding PEG as surfactant and dispersant. Notably PEG addition increased the BET surface area of materials and prevented the coagulation of particles in materials. The active metal dispersion and OSC of this catalyst ranked at the top of the series catalysts. The weight ratio of Ni to Zr was much higher than that of the designed composition. As proven by CO pulse chemisorptions results, more Ni and Co active sites were present on the surface than inside the catalyst. Raman spectroscopy confirmed that more oxygen vacancies and defects were present in 15Ni— 5Co/$Ce_{0.75}Zr_{0.25}O_2$—P5 catalyst. Similarly, the oxygen vacancies and defects in catalytic structure increased after its H_2-treatment. The reduction treatment at high temperature partially reduces the support, generating oxygen vacancies and Ce^{3+} cations close to the active metal particles that can electronically modify the catalytic behavior of the active metal. Thus, the oxygen vacancies are important for the catalyst performance.[39] Oxygen vacancies and defects can activate and cause CO_2 (ad) and H_2 molecules to dissociate more easily.[40] Zr^{4+} cations replace Ce^{4+} cations in the CeO_2 lattice in the catalyst to make the Ce^{4+} cations easily reduced into Ce^{3+}. The presence of more Ce^{3+} increases the adsorption capacity of the catalyst for H atoms produced by dissociative adsorption of H_2 on the dispersed active metals and spillover onto the mixed oxide support surface, resulting in higher catalytic activities.[41]

Conclusion

CO_2 methanation was performed over a series of active oxygen material $Ce_xZr_{1-x}O_2$ supported Ni—Co bimetallic nanosized catalysts prepared by coprecipitation method. The interaction between active metals (Ni and Co) and $Ce_xZr_{1-x}O_2$ support significantly affected the catalytic activity. The CeO_2/ZrO_2 ratio affected the catalytic performance by obtaining more oxygen vacancies and inducing structural changes. Appropriate Co metal addition can improve catalytic stability of catalysts significantly. PEG-6000 addition can increased the BET surface area, active metal dispersion, and oxygen vacancies, which all contribute to higher activity. Oxygen vacancies close to the active metal particles can electronically modify the catalytic behavior of the active metal particles. Oxygen vacancies and defects can activated and induced CO_2 (ad) and H_2 molecules to dissociate more easily. Thus, the nanosized catalyst 15 wt % Ni—5 wt % Co— $Ce_{0.25}Zr_{0.75}O_2$ adding 5 wt % PEG-6000 can result in 85% CO_2 conversion and 98% selectivity to methane at 280°C.

Acknowledgments

The authors gratefully acknowledge financial support from the National Natural Science Foundation of China (No. 21006113), the National Basic Research Program of China (No. 2009CB219900), and the National High Technology Research and Development Program of China (No. 2011AA050606).

Literature Cited

1. Zhang ZH, Ma XL, Wang DX, Song CS, Wang YG. Development of silica-gel-supported polyethylenimine sorbents for CO_2 capture from flue gas. *AIChE J*. 2011;58:2495–2502.
2. Monazam ER, Shadle LJ, Pennline H, Fauth D, Miller DC, Hoffman JS, Gray ML. Equilibrium and kinetics analysis of carbon dioxide capture using immobilized amine on a mesoporous silica. *AIChE J*. 2012; DOI:10.1002/aic.13870.
3. Huang W, Sun WZ, Li F. Efficient synthesis of ethanol and acetic acid from methane and carbon dioxide with a continuous, stepwise reactor. *AIChE J*. 2010;56:1279–1284.
4. Park JN, McFarland EW. A highly dispersed Pd–Mg/SiO_2 catalyst active for methanation of CO_2. *J Catal*. 2009;266:92–97.
5. Govender NS, Botes FG, Schouten JC. Mechanistic pathway for methane formation over an iron-based catalyst. *J Catal*. 2008;260: 254–261.
6. Sharma S, Hu ZP, Zhang P, McFarland EW, Metiu H. CO_2 methanation on Ru-doped ceria. *J Catal*. 2011;278:297–309.
7. Mao TF, Falconer JL. Methanation sites on a Pt/TiO_2 catalyst. *J Catal*. 1990;123:443–455.
8. Aksoylua AE, Akina AN, Önsana Zİ, Trimm DL. Structure/activity relationships in coprecipitated nickel-alumina catalysts using CO_2 adsorption and methanation. *Appl Catal A*. 1996;145:185–193.
9. Du GA, Lim SY, Yang YH, Wang C, Pfefferle L, Haller GL. Methanation of carbon dioxide on Ni-incorporated MCM-41 catalysts: the influence of catalyst pretreatment and study of steady-state reaction. *J Catal*. 2007;249:370–379.
10. Zhi GJ, Guo XN, Wang YY, Jin GQ, Guo XY. Effect of La_2O_3 modification on the catalytic performance of Ni/SiC for methanation of carbon dioxide. *Catal Commun*. 2011;16:56–59.
11. Kim JR, Myeong WJ, Ihm SK. Characteristics of CeO_2–ZrO_2 mixed oxide prepared by continuous hydrothermal synthesis in supercritical

water as support of Rh catalyst for catalytic reduction of NO by CO. *J Catal*. 2009;263:123–133.
12. Zhao MW, Shen MQ, Wang J. Effect of surface area and bulk structure on oxygen storage capacity of $Ce_{0.67}Zr_{0.33}O_2$. *J Catal*. 2007;248:258–267.
13. Abdollahzadeh-Ghom S, Zamani C, Andreu T, Epifani M, Morante JR. Improvement of oxygen storage capacity using mesoporous ceria–zirconia solid solutions. *Appl Catal B*. 2011;108–109:32–38.
14. Widmann D, Leppelt R, Behm RJ. Activation of a Au/CeO_2 catalyst for the CO oxidation reaction by surface oxygen removal/oxygen vacancy formation. *J Catal*. 2007;251:437–442.
15. Zhu HW, Razzaq R, Jiang L, Li CS. Low-temperature methanation of CO in coke oven gas using single nanosized Co_3O_4 catalysts. *Catal Commun*. 2012;23:43–47.
16. Ocampo F, Louis B, Roger AC. Methanation of carbon dioxide over nickel-based $Ce_{0.72}Zr_{0.28}O_2$ mixed oxide catalysts prepared by sol–gel method. *Appl Catal A*. 2009;369:90–96.
17. Ocampo F, Louis B, Kiwi-Minskerb L, Roger AC. Effect of Ce/Zr composition and noble metal promotion on nickel based $Ce_xZr_{1-x}O_2$ catalysts for carbon dioxide methanation. *Appl Catal A*. 2011;392:36–44.
18. Khodakov AY, Griboval-Constant A, Bechara R, Zholobenko VL. Pore size effects in Fischer Tropsch synthesis over cobalt-supported mesoporous silicas. *J Catal*. 2002;206:230–241.
19. Prieto G, Martínez A, Concepción P, Tost RM. Cobalt particle size effects in Fischer–Tropsch synthesis: structural and in situ spectroscopic characterisation on reverse micelle-synthesised Co/ITQ-2 model catalysts. *J Catal*. 2009;266:129–144.
20. Wang T, Ding YJ, Lü Y, Zhu HJ, Lin LW. Influence of lanthanum on the performance of Zr-Co/activated carbon catalysts in Fischer-Tropsch synthesis. *J Nat Gas Chem*. 2008;17:153–158.
21. Hu CQ, Zhu QS, Jiang Z. Nanosized $CuO\text{-}Zr_xCe_{1-x}O_y$ aerogel catalysts prepared by ethanol supercritical drying for catalytic deep oxidation of benzene. *Powder Technol*. 2009;194:109–114.
22. Wei ZL, Li HM, Zhang XY, Yan SH, Lv Z, Chen YQ, Gong MC. Preparation and property investigation of $CeO_2\text{-}ZrO_2\text{-}Al_2O_3$ oxygen-storage compounds. *J Alloys Compd*. 2008;455:322–326.
23. Krämer M, Stöwe K, Duisberg M, Müller F, Reiser M, Sticher S, Maier WF. The impact of dopants on the activity and selectivity of a Ni-based methanation catalyst. *Appl Catal A*. 2009;369:42–52.
24. Wang YZ, Wu RF, Zhao YX. Effect of ZrO_2 promoter on structure and catalytic activity of the Ni/SiO_2 catalyst for CO methanation in hydrogen-rich gases. *Catal Today*. 2010;158:470–474.
25. Maia TA, Assaf JM, Assaf EM. Steam reforming of ethanol for hydrogen production on $Co/CeO_2\text{–}ZrO_2$ catalysts prepared by polymerization method. *Mater Chem Phys*. 2012;132:1029–1034.
26. McBride JR, Hass KC, Poindexter BD, Weber WH. Raman and X-ray studies of $Ce_{(1-x)}$ $RE_{(x)}$ $O_{(2-y)}$, where RE=La, Pr, Nd, Eu, Gd, and Tb. *J Appl Phys*. 1994;76:2435–2441.
27. Liu ZG, Zhou RX, Zheng XM. Influence of residual K^+ on the catalytic performance of $Cu\text{-}CeO_2$ catalysts in preferential oxidation of CO in excess hydrogen. *Int J Hydrogen Energy*. 2008;33:791–796.
28. Wang H, Zhu HQ, Qin ZF, Liang FX, Wang GF, Wang JG. Deactivation of a $Au/CeO_2\text{–}Co_3O_4$ catalyst during CO preferential oxidation in H_2-rich stream. *J Catal*. 2009;264:154–162.
29. Liu Q, Wang LC, Chen M, Cao Y, He HY, Fan KN. Dry citrate-precursor synthesized nanocrystalline cobalt oxide as highly active catalyst for total oxidation of propane. *J Catal*. 2009;263:104–113.
30. Rossignol S, Gérard F, Duprez D. Effect of the preparation method on the properties of zirconia-ceria materials. *J Mater Chem*. 1999;9:1615–1620.
31. Rossignol S, Madier Y, Duprez D. Preparation of zirconia–ceria materials by soft chemistry. *Catal Today*. 1999;50:261–270.
32. Fornasiero P, Dimonte R, Rao GR, Kašpar J, Meriani S, Trovarelli A, Graziani M. Rh-loaded $CeO_2\text{–}ZrO_2$ solid solutions as highly efficient oxygen exchangers: dependence of the reduction behavior and the oxygen storage capacity on the structural properties. *J Catal*. 1995;151:168–177.
33. Zhang YW, Wen J, Wang J, Pan DC, Shen MQ, Lu YF. Synthesis of monodisperse $Ce_xZr_{1-x}O_2$ nanocrystals and the size-dependent enhancement of their properties. *Nano Res*. 2011;4:494–504.
34. Takaaki T, Tomoaki W, Nobuhiro M, Masahiro Y. Hydrothermal synthesis of monodisperse $Ce_{0.5}Zr_{0.5}O_2$ metastable solid solution nanocrystals. *Eur J Inorg Chem*. 2009;14:2054–2057.
35. Lin XM, Li LP, Li GS, Su WH. Transport property and Raman spectra of nanocrystalline solid solutions $Ce_{0.8}Nd_{0.2}O_{2-\delta}$ with different particle size. *Mater Chem Phys*. 2001;69:236–240.
36. Li GF, Wang QY, Zhao B, Zhou RX. A new insight into the role of transition metals doping with $CeO_2\text{–}ZrO_2$ and its application in Pd-only three-way catalysts for automotive emission control. *Fuel* 2012;92:360–368.
37. Takanabe K, Nagaoka K, Nariai K, Aika K. Titania-supported cobalt and nickel bimetallic catalysts for carbon dioxide reforming of methane. *J Catal*. 2005;232:268–275.
38. Luisetto I, Tuti S, Bartolomeo ED. Co and Ni supported on CeO_2 as selective bimetallic catalyst for dry reforming of methane. *Int J Hydrogen Energy*. 2012;37:15992–15999.
39. Li CS, Hirabayashi D, Suzuki K, A crucial role of $O^{2}\_$ and $O_2{}^{2}\_$ on mayenite structure for biomass tar steam reforming over $Ni/Ca_{12}Al_{14}O33$. *Appl Catal B*. 2009;88:351–360.
40. Zhang RG, Wang BJ, Ling LX, Liu HY, Huang W. Adsorption and dissociation of H_2 on the $Cu_2O(1\ 1\ 1)$ surface: a density functional theory study. *Appl Surf Sci*. 2010;257:1175–1180.
41. Pokrovski KA, Rhodes MD, Bell AT. Effects of cerium incorporation into zirconia on the activity of Cu/ZrO_2 for methanol synthesis via CO hydrogenation. *J Catal*. 2005;235:368–377.

Manuscript received July 12, 2012, and revision received Dec. 19, 2012.